Convective Momentum Transport over the Tropical Pacific: Budget Estimates

MATTHEW T. CARR AND CHRISTOPHER S. BRETHERTON

Department of Atmospheric Sciences, University of Washinton, Seattle, Washington

(Manuscript received 17 February 2000, in final form 11 October 2000)

ABSTRACT

ECMWF and NCEP–NCAR reanalyses are used to calculate convective momentum transport (CMT) as a momentum budget residual over several tropical oceanic convective regions, including the TOGA COARE Intensive Flux Array (IFA). Sources of uncertainty are quantified through intercomparison, and methods for minimizing uncertainty are discussed. The authors examine how the environmental shear of the time-mean, and time-varying, flow in these regions is modified by CMT, and compare the budget results with some parameterizations.

The zonal residual is a significant term in the time-mean reanalysis budgets in all regions below 850 mb. Since the subcloud turbulent layer typically does not extend above 940 mb, this suggests a possibly important role for CMT by shallow convection. In the rest of the troposphere, the residuals are small, but a slight tendency for downgradient transport of zonal momentum, and smoothing of the environmental wind profile, is suggested. The main budget uncertainties associated with pressure gradient forces and horizontal advection are substantially reduced by considering a larger domain, and by averaging over long periods. The Gregory et al. CMT parameterization scheme shows qualitative agreement with the time-mean budget residuals in all regions above 850 mb. The Schneider and Lindzen scheme shows poorer agreement. Neither parameterization captures the residual accelerations seen below 850 mb.

1. Introduction

Deep and shallow cumulus convection frequently occurs in environments of large vertical wind shear. In these environments, convective updrafts may have a systematically different horizontal velocity than convective downdrafts, resulting in a net vertical flux of horizontal momentum, or convective momentum transport (CMT). Studies of both idealized (e.g., Houze 1973; Schneider and Lindzen 1977), and general circulation (e.g., Inness and Gregory 1999; Zhang and McFarlane 1995), models have suggested that CMT has a significant effect on mean zonal winds in the Tropics, and may also play a role in transient disturbances such as the Madden–Julian oscillation (MJO). However, few reliable observations exist over regions large enough to verify these modeling results.

Consequently, treatment of CMT varies widely among cumulus parameterizations used in large-scale circulation models. The National Center for Atmospheric Research Community Climate Model (CCM3) neglects cumulus momentum fluxes entirely (Kiehl et al. 1996). The Kain–Fritsch (1990) scheme treats momentum like a scalar, while others (e.g., Wu and Yanai 1994; Kershaw and Gregory 1997; Tiedtke 1993; Zhang and Cho 1991a,b) represent the effects of local pressure perturbations and entrainment on cloud momentum.

One fundamental question that remains unanswered is the importance of mesoscale storm organization to CMT. Most current CMT parameterizations are based on idealized models of flow entrained into and diverted around an isolated cumulus updraft. These parameterizations tend to produce downgradient fluxes (i.e., momentum is fluxed from levels with higher horizontal velocity to levels with lower horizontal velocity), which results in a smoothing of the environmental wind profile.

Direct (eddy correlation) estimates of cumulus momentum fluxes have been made using aircraft and Doppler radar data. In a seminal observational study of momentum fluxes in squall lines, LeMone (1983) showed that in the across-line direction, momentum fluxes can act to increase the environmental wind shear. The tilt of the updraft produced mesoscale horizontal pressure gradients around the leading edge of the line that accelerated the updrafts rearward and downdrafts forward. This pressure distribution is exactly opposite to that predicted by flow around an obstacle, and suggests that cumulus momentum fluxes can depend considerably on the convective organization.

These results have been confirmed in many observational studies of squall lines (e.g., LeMone et al. 1984; Flatau and Stevens 1987; LeMone and Jorgenson 1991;

Corresponding author address: Matthew Carr, Dept. of Atmospheric Sciences, University of Washington, Box 351640, Seattle, WA 98195.
E-mail: tobias@atmos.washington.edu

Gallus and Johnson 1992), and in several modeling studies (e.g., Soong and Tao 1984; LaFore et al. 1988; Gao et al. 1990). To account for these observations, Moncrieff (1992) developed an archetypal model that allows for countergradient transport in organized convection. LeMone and Moncrieff (1993) found that this model was the most appropriate representation of line-normal CMT for quasi-two-dimensional convective bands. However, in a 3D numerical study that included the ends of a squall line, Trier et al. (1998) found that the overall cross-line CMT was downgradient, even though it was upgradient on the midplane.

These studies, while illuminating, are limited to a few individual systems. An alternative approach is to derive momentum flux convergence as the residual of the horizontal momentum budget from an objective analysis. This method is appealing because of its simplicity and the widespread availability of large-scale radiosonde observations of winds and geopotential height. It also has the advantage that it reveals the ensemble effect of all convection in a region under a variety of conditions. However, budget residual calculations of CMT are prone to large uncertainties, especially for deep convection.

Momentum budgets have been constructed both for shallow convection (e.g., Holland and Rasmussen 1973) and deep convection (e.g., Stevens 1979; Wu and Yanai 1994). Holland and Rasmussen calculated a 5-day-average momentum budget for a quasi-steady trade cumulus boundary layer during the Barbados Oceanographic and Meteorologic Experiment (BOMEX), in a region surrounded by four ships taking frequent soundings. The flow steadiness, high quality, and frequency of soundings made for a particularly believable budget residual that agrees well with large-eddy simulations of this case (Brown 1999). The implied momentum flux convergence was mainly in the subcloud layer, but there were also significant fluxes in the lower half of the cumulus layer.

Stevens (1979) calculated the momentum budget in easterly waves over the tropical Atlantic Ocean, in which deep convection was often organized into north–south oriented squall lines. In the wave troughs, where convection was most vigorous, Stevens found downgradient CMT in the along-line direction with little CMT in the across-line direction, an anisotropy consistent with in situ observations of squall lines. The synoptic-scale pressure gradient force was a major uncertainty in this study.

Wu and Yanai (1994) examined mesoscale convective systems observed by storm-scale and mesoscale sounding arrays in Oklahoma and Kansas. Upper-tropospheric environmental wind shear was reduced by CMT in a mesoscale convective complex case and increased in a squall line case, again suggesting a relationship between CMT and convective organization. Sui and Yanai (1986) calculated the curl of the momentum flux convergence as a budget residual in the vorticity equation. They found downgradient momentum fluxes in most of the tropical Atlantic convective systems they analyzed.

In this work, we assess whether cumulus momentum fluxes can be reliably determined from global reanalysis datasets, and assess two parameterizations of CMT in light of our findings. Reanalyses use modern analysis and forecast systems to assimilate global observational data over long periods. Their sweeping spatial and temporal coverage gives them the potential to provide unprecedented insight into the role of CMT in global circulations.

However, the use of reanalysis data also has several limitations. The coarse resolution (both spatial and temporal) afforded by global analyses is unable to resolve sporadic and localized convective events, which may be important to the large-scale flow. While reanalyses will not resolve the effects of individual systems, these datasets should be sufficient to resolve the systematic effects of convection, which are of primary importance to global models.

In addition, it must be kept in mind that these ''observations'' contain some component that depends on the characteristics of the model used in the reanalysis. In this paper we examine to what extent these characteristics play a role in reanalysis momentum budgets by comparing two models with considerably different physics, including their cumulus parameterizations. Similarities between the two models may be indicative of a real signal in the observations.

The Tropical Ocean Global Atmosphere Coupled Ocean–Atmosphere Response Experiment (TOGA COARE; Webster and Lukas 1992) provides an attractive opportunity to examine reanalysis-based estimates of CMT. A model-free objective analysis derived from the experiment's extensive observational network is available for the TOGA COARE domain. Furthermore, during ''active'' periods of strong deep convection, there was often strong, deep vertical wind shear, lending hope that cumulus momentum fluxes might be sufficiently large to reliably estimate from a budget approach.

This study is organized as follows. In section 2, we describe the momentum budget approach. In section 3, we construct time-mean and time-varying momentum budgets using observations from TOGA COARE. We look at three independent analyses in order to obtain an estimate of the uncertainty in the terms of the momentum budget. In section 4, we construct budgets for other tropical oceanic regions. In section 5, we compare budget results with existing parameterizations of cumulus momentum transport. Section 6 offers a summary and discussion of our results.

2. The momentum budget approach

We examine the COARE intensive flux array (IFA; Fig. 1) during the intensive observation period (IOP; November 1992 to February 1993). During this period soundings were launched ever 6 h at four stations on

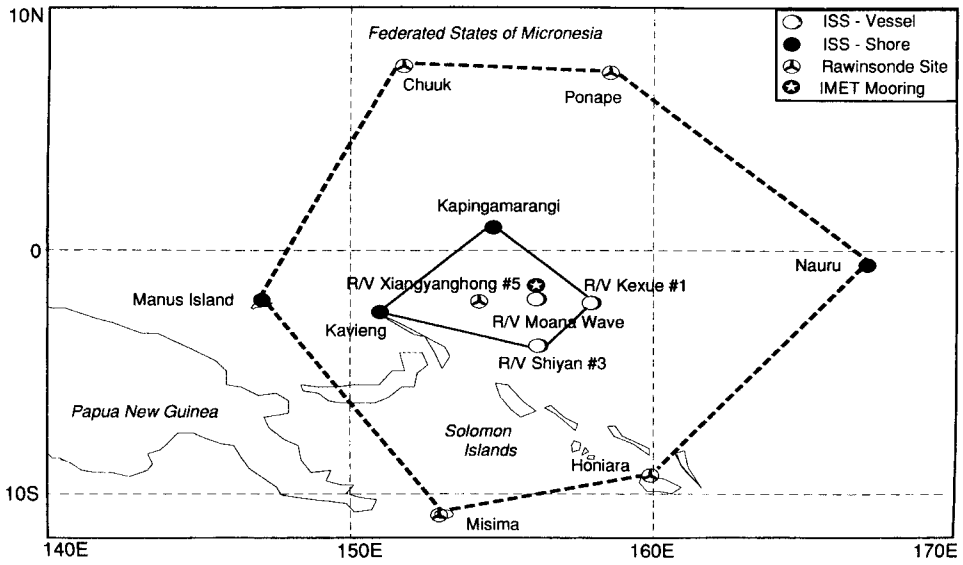

FIG. 1. Map of TOGA COARE region. Boundary of IFA given by dark solid lines. Boundary of outer sounding array given by dark dashed lines. Sounding stations indicated by circles.

the perimeter of the IFA: Kavieng (2.35°S, 150.48°E), Kapingamarangi (1.04°N, 154.48°E), R/V *Kexue#1* (4.00°S, 156.00°E), and R/V *Shiyan#3* (2.00°S, 158.00°E). Soundings were also taken at a more coarsely spaced network of surrounding stations.

The zonal momentum equation can be written (e.g., Stevens 1979)

$$X = \frac{\partial u}{\partial t} + \mathbf{v} \cdot \nabla_p u + \omega \frac{\partial u}{\partial p} - f(y)v + \frac{\partial \varphi}{\partial x}. \quad (1)$$

Here $\mathbf{v}$ is the horizontal vector wind, ∇_p the horizontal gradient operator applied at constant pressure, u the zonal wind, v the meridional wind, and ω the vertical pressure velocity; x and y are E–W and N–S distance, f the Coriolis parameter, and φ geopotential height.

Here X represents accelerations due to all subgrid-scale processes. In the free troposphere (above the effects of boundary layer turbulent eddies), over the open ocean (away from the effects of topographically induced gravity waves), it is reasonable to assume that CMT is the dominant subgrid-scale process responsible for the vertical transport of momentum.

Under this assumption, we can write

$$X = \frac{\partial}{\partial p}\overline{u'\omega'}, \quad (2)$$

where the overbar denotes an ensemble average at a given pressure level, and primes denote the local perturbation from the ensemble average. In this way, we define X to be the acceleration of the zonal flow due to the convergence of zonal momentum flux, $\overline{-u'\omega'}(p)/g$. (Here we use g, gravitational acceleration, as a scaling factor to give the momentum flux in its most common units, pascals; the negative sign defines upward fluxes of westerly momentum to be positive.) Analogous formulas give Y, acceleration of the meridional flow by meridional momentum flux convergence.

The momentum flux at any level is then obtained by integrating upward from the surface:

$$\overline{u'\omega'}(p) = \overline{u'\omega'}_{\text{sfc}} - \int_p^{p_{\text{sfc}}} X(p)\, dp. \quad (3)$$

The subscript sfc indicates the surface value. The zonal component of the surface wind stress vector, $\overline{-u'\omega'}_{\text{sfc}}/g$, which is estimated from buoy data, is used as a lower boundary condition. Analogous formulas give the meridional momentum flux, $\overline{-v'\omega'}(p)/g$.

In addition to other unresolved accelerations, the residuals also contain any errors due to the observed wind and pressure fields. In previous studies (e.g., Stevens 1979), errors in the pressure fields (which may be due to errors in measured surface pressure or in hydrostatic calculations of layer thickness) have been the largest obstacle. The quantity of data and the length of the record from TOGA COARE lend hope for more conclusive results.

Use of the advective form (1) for calculating residuals may also introduce additional errors in the reanalysis budgets due to discrepancies between spatial differences computed by the model, and those calculated in the budget. The National Centers for Environmental Prediction–National Center for Atmospheric Research (NCEP–NCAR) reanalysis was performed on sigma levels and subsequently transformed to the pressure level data we used. NCEP also used a spectral advection algorithm. Thus, it was not possible to maintain complete consistency between our numerical approach and that used in the reanalysis itself. However, in spatial averaging over all grid points in the IFA, random errors

should be reduced. Also, there is no nearby orography to produce systematic errors in our differencing approach.

A simple consistency check on the residual calculation is to assume that upward momentum fluxes at the tropopause are typically much smaller than their corresponding surface values. Hence, from (3),

$$\overline{u'\omega'}_{\text{sfc}} \approx \int_{p_T}^{p_{\text{sfc}}} X(p), \tag{4}$$

where subscript T denotes the tropopause value. A similar approximation holds for meridional across-tropopause fluxes. We justify this assumption with an estimate of the upward momentum fluxes into the stratosphere required to produce the quasi-biennial oscillation (QBO).

The maximum zonally averaged accelerations associated with the descent of the QBO are about 30 m s^{-1} in 1 month over a 20-mb depth of the stratosphere (e.g., Fig. 12.11 of Holton 1992). Such accelerations would be produced by an upward momentum flux of 2×10^{-3} Pa across the tropopause absorbed over the 20-mb layer. In contrast, typical surface fluxes are 10^{-2}–10^{-1} Pa. Hence, even if only 10% of the cumulus momentum flux across the tropopause goes to drive the QBO, the largest fluxes at this level should be no larger than the typical surface flux. Across-tropopause fluxes much larger than the surface flux indicate the presence of errors in the budget residual.

We construct momentum budgets for three different analyses of the IOP. We examine the objective analysis of Ciesielski et al. [(1997, hereafter CJ); analysis available online from the Colorado State University Web site: http://tornado.atmos.colostate.edu/togadata], the NCEP–NCAR, global reanalysis [Kalney et al. (1996); analysis available online from the Climate Diagnostics Center Web site: http://www.cdc.noaa.gov/cdc/data.nmc.reanalysis.html], and the European Centre for Medium-Range Weather Forecasts (ECMWF) global reanalysis [Gibson et al. (1997); analysis available online from the University Cooperation for Atmospheric Research Web site: http://dss.ucar.edu/pub/ec-reanalysis.html]. Grid spacing is 1° in both the zonal and meridional directions in CJ and 2.5° in NCEP and ECMWF. Daily-averaged (NCEP) or 6-h-averaged (CJ, ECMWF) residuals were calculated at each grid point within the IFA, then spatially averaged to give IFA mean profiles.

The area-average quantities should be independent of the different spatial resolutions, since most of the information used in the analyses was obtained at the vertices of, and outside, the IFA.[1] Also, considerable temporal averaging was required to obtain robust results, as discussed in the following section. This averaging should remove differences due to temporal resolution.

3. Results of TOGA COARE budget

Figure 2 shows the evolution of the ECMWF zonal wind and CJ precipitation averaged over the IFA region during the IOP. The period is characterized by two episodes of strong low-level westerlies, generally referred to as westerly wind burst (WWB) events. The events peak on Julian days 367 and 400. (Day 001 corresponds to 1 January 1992). Maximum 5-day-running-mean 750-mb winds during the WWBs are in excess of 14 and 12 m s^{-1}, respectively. Precipitation maxima were observed during the onset of both events.

We begin in section 3a by examining the momentum budget time-averaged over the 4-month IOP. Next we examine the time-varying profiles. In section 3b we focus on the strongest variability, and filter any errors in the time-mean fields, by adopting a compositing approach based on an empirical orthogonal function (EOF) analysis of the wind profile. This provides the profiles of u and v that explain the greatest variance, and the corresponding budget residuals. In section 3c we evaluate the uncertainty in the budget terms, and in section 3d we examine time series of u and X smoothed with a 5-day running-mean filter. These time series preserve the low-frequency variability while filtering the noise associated with higher frequencies.

a. Time-mean momentum budget

Figure 3 gives the profiles of the zonal and meridional components of the horizontal wind averaged over the 4-month period from each of the analyses. The three analyses are (as one would hope) nearly identical, with mean westerlies below 500 mb and mean easterlies above. The time-mean meridional wind is less than 2 m s^{-1} at all levels.

Figure 4 contains profiles of the terms on the right-hand side of the zonal momentum equation (1) averaged over the same period. The local time rate of change term, $\partial u/\partial t$, is omitted, but is nearly zero at all levels in the 4-month mean. Also shown is an estimate of the random uncertainty in these terms described in section 3c.

The time-mean Coriolis force and horizontal advection agree well between the three analyses. Differences between the analyses are generally within the random uncertainty for these terms. However, there are substantial differences in vertical advection and the pressure gradient force.

The differences in vertical advection are due at least in part to large differences in the time-mean vertical velocity (Fig. 5). The mean upward motion in both reanalysis products is much weaker than is seen in the CJ objective analysis. The CJ vertical velocities are cal-

[1] The difference in gridpoint spacing between the objective analyses and the reanalyses did result in a systematic difference in the calculated area-average Coriolis force (see Fig. 5). The higher resolution of the CJ analysis included more grid points in the southern portion of the IFA (Fig. 1). These southern latitudes were thus weighted more heavily in the CJ analysis. However, this discrepancy was small compared with differences in other terms of the budget.

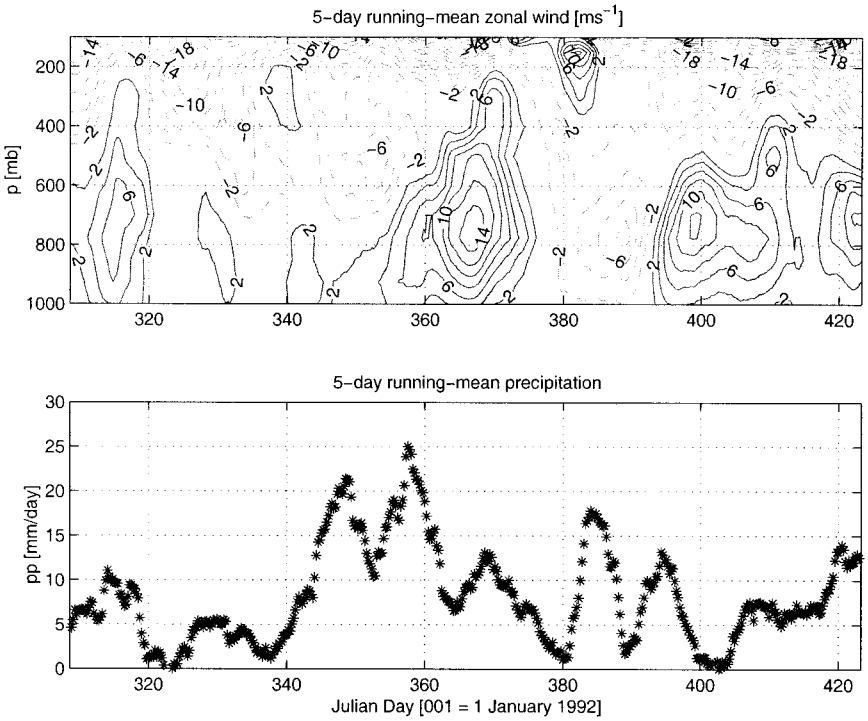

FIG. 2. Five-day-running-mean zonal wind from ECMWF, and precipitation from Ciesielski et al. (1997). Solid lines indicate westerly winds; dashed lines are easterlies.

culated by integration of the mass continuity equation from the surface to the tropopause (Lin and Johnson 1996), using winds observed at the corners of the IFA. A constant adjustment was applied to the vertical distribution of divergence, with the vertical velocity set to zero at 75 mb.

The reanalysis vertical velocities, on the other hand, depend on the location and timing of the convection in the model, among other factors. Examining the mean precipitation rates during the IOP (not shown), it appears the reanalyses are producing too little convection in the IFA region. The average precipitation rate during the 4-month IOP is 8.2 mm day^{-1} in the objective analysis (Lin and Johnson 1996). In the NCEP and ECMWF reanalyses the average precipitation rates are 7.7 and 5.9 mm day^{-1}, respectively. It is possible the reanalyses are enhancing convection in the intertropical convergence zone (ITCZ) or the South Pacific convergence zone at the expense of convection over the IFA. Differences in the time evolution of the vertical velocity (see Fig. 8d) may also be contributing to differences in vertical advection.

The largest discrepancy among the analyses is in the pressure gradient term. The CJ analysis exhibits stronger pressure accelerations through most of the troposphere than either of the reanalyses in the 4-month mean. The differences are even more pronounced in the meridional budget (Fig. 6), where the CJ pressure term is an order

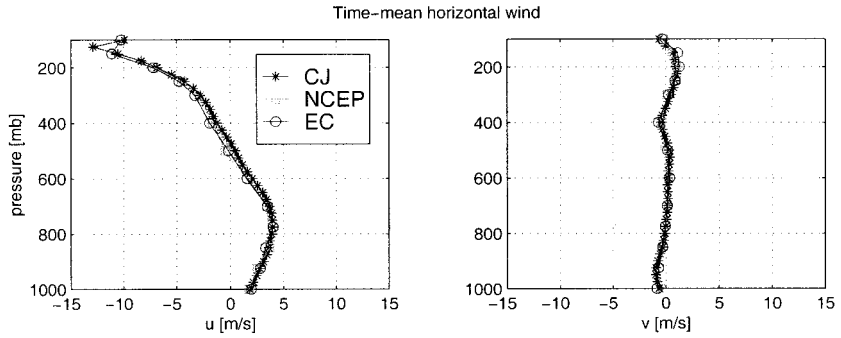

FIG. 3. Time-mean zonal and meridional wind components averaged over COARE IFA during IOP.

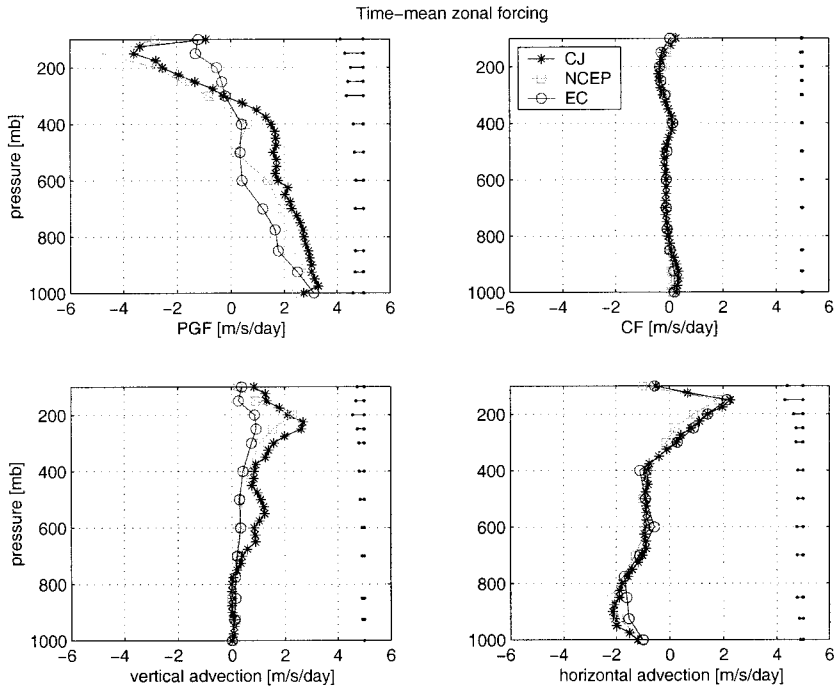

FIG. 4. Terms of time-mean zonal momentum budget averaged over IFA during IOP. (clockwise from upper left) Pressure gradient force; Coriolis force; horizontal advection; and vertical advection. Error bars indicate 1 std dev difference between NCEP and ECMWF.

of magnitude larger than the reanalyses. The other terms in the meridional budget show good agreement.[2]

Figure 7 gives the time-mean budget residuals for the IFA region from (1), and the corresponding implied momentum flux profiles. The CJ zonal and meridional residuals are negative throughout the troposphere. Integrating vertically, they imply upward momentum fluxes through the tropopause much greater than the surface drag. This violates the consistency check outlined in section 2.

The large residuals in the CJ analysis are the result of the large unbalanced pressure gradient terms. The consistency check demonstrates that the CJ pressure gradient terms are probably in error. One apparent cause is an error in the surface pressure used for initializing the radiosonde ascents at R/V *Kexue #1* (P. Ciesielski 1998, personal communication).

The surface pressure errors appear to be due to the use of a poorly calibrated barometer. Surface pressure errors are translated through the depth of the atmosphere, since geopotential heights are computed using the hydrostatic equation. Presumably the reanalyses (which include as input all upper-air data taken during TOGA COARE) rejected this sounding station, resulting in more realistic pressure fields.

In light of the large pressure errors in the objective analysis we focus on the reanalyses. The time-mean zonal residuals from the reanalyses look quite similar. However, there are large differences between the time-mean reanalysis meridional budget residuals. The NCEP budget has $Y < 0$ through most of the troposphere, which gives an implied upward meridional momentum flux of approximately 0.1 Pa across the tropopause. This is an order of magnitude larger than the surface drag and suggests an inconsistency in the NCEP analysis. The source of the error again appears to be in the an-

[2] Recall the difference between the CJ Coriolis force and the reanalysis Coriolis forces is due to the difference in gridpoint spacing.

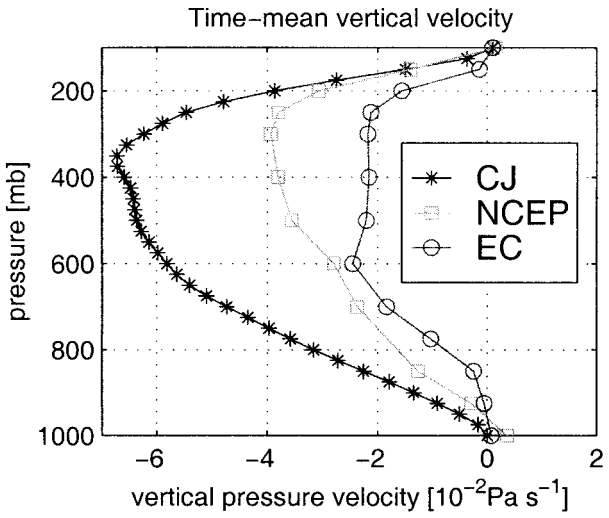

FIG. 5. Time-mean vertical pressure velocity averaged over IFA during IOP. Negative values indicate upward motion.

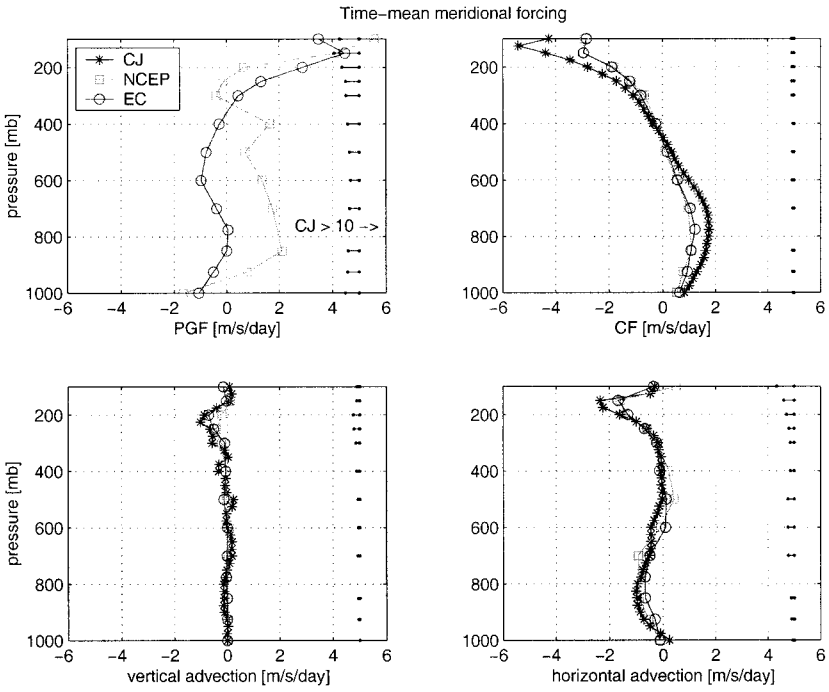

FIG. 6. Terms of time-mean meridional momentum budget averaged over IFA during IOP. (clockwise from upper left) Pressure gradient force; Coriolis force; horizontal advection; and vertical advection. Error bars indicate 1 std dev difference between NCEP and ECMWF.

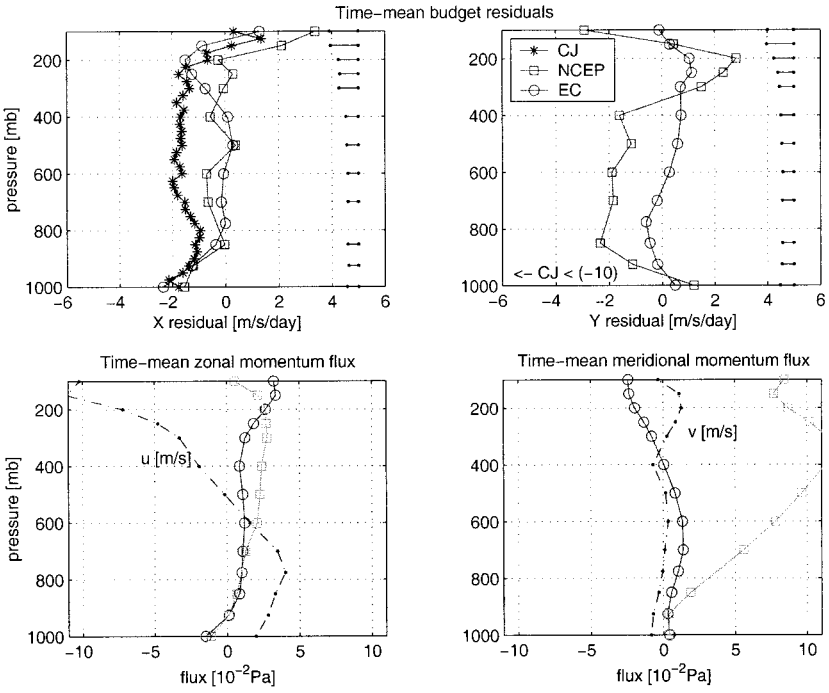

FIG. 7. (top) Time-mean zonal and meridional budget residuals, averaged over IFA during IOP. Error bars indicate 1 std dev difference between NCEP and ECMWF. (bottom) Time-mean zonal and meridional wind components and momentum flux, averaged over IFA during IOP. Positive values indicate upward flux of westerly/southerly momentum.

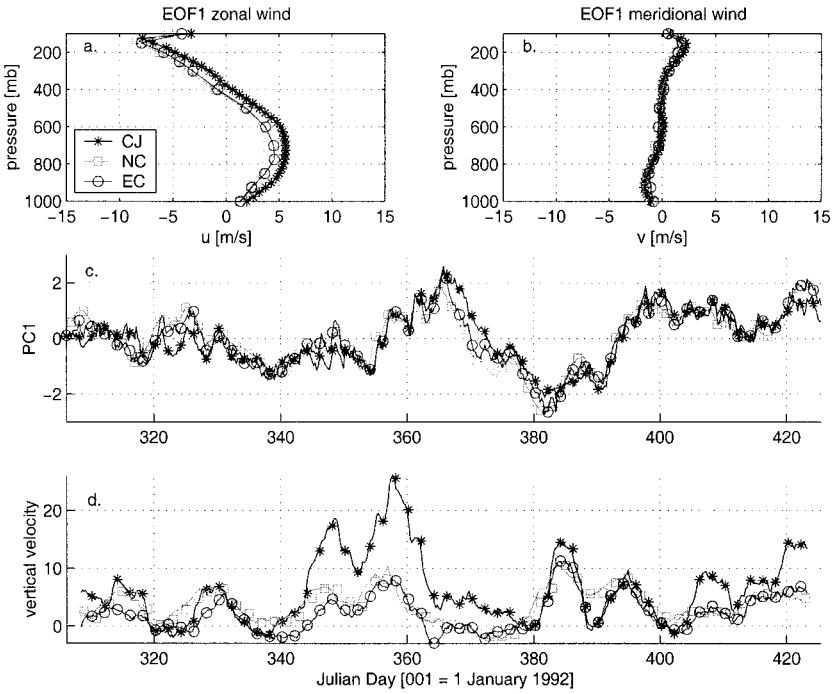

FIG. 8. (a) Zonal component of EOF1 of vector wind averaged over IFA during IOP; (b) meridional component; (c) corresponding principal component time series; (d) 500-mb vertical velocity in 10^{-2} Pa s^{-1} (positive values indicate upward motion), smoothed with 5-day-running-mean filter. (Data are plotted at 2-day intervals for clarity.)

alyzed height fields. The NCEP analysis exhibits a persistent unbalanced northward-directed pressure gradient across the IFA (Fig. 6). This may result from blending of the erroneous *Kexue #1* surface pressures into the reanalysis.

The implied flux profiles from the ECMWF reanalysis are more reasonable. Fluxes deduced from the residual are comparable in magnitude to the surface drag through the depth of the troposphere. Fluxes increase above the tropopause, which suggests there may still be significant errors in the observed fields.

The presence of random and systematic errors preclude the identification of a CMT signal at any level in the time-mean meridional budget. The ECMWF meridional residual, *Y,* is essentially indistinguishable from zero through the depth of the troposphere. The time-mean zonal residual, *X,* is also indistinguishable from zero through most of the troposphere. However, *X* is clearly a significant term in the budget below 850 mb (Fig. 7), with accelerations up to 2 m s^{-1} day^{-1} in both reanalyses. These low-level accelerations are comparable in magnitude to the largest forcing terms (Fig. 4). The ECMWF zonal residual is also comparable to the other forcing terms in the upper troposphere. However, at these levels the random uncertainty is quite large.

Given the uncertainties in the budget residuals, the character of the momentum fluxes above 850 mb cannot be unambiguously determined. However, if correct, the zonal momentum flux profiles in Fig. 7 suggest down-gradient transport at most levels in the 4-month average.

b. Time-varying momentum budget—EOF analysis

We now consider the time-varying part of the momentum budget. In this section, our goal is to isolate the CMT variations associated with the oscillation between low-level easterlies and westerlies during the IOP, while averaging out most of the random uncertainty in the budget terms. To do this, we calculate the residuals associated with the leading principal component (PC1) of the first EOF of the IFA vector wind profile.

The first EOF of the vector wind (Figs. 8a,b) has a similar profile to the mean wind. It explains 37% of the total variance in the vector wind in the CJ analysis, 41% in the NCEP reanalysis, and 28% in ECMWF. The EOF has been normalized to correspond to a 1 standard deviation anomaly of the corresponding principal component from its time mean.

A time series of the standardized PC1 from each of the analyses is given in Fig. 8c. The strongest signal is at 30–60-day periods, associated with the MJO. PC1 is greatest during the two WWBs. The onset of these WWBs is associated with active phases of the MJO, as seen in the time series of 500 mb vertical velocities (Fig. 8d). Thus PC1-regressed profiles give a composite

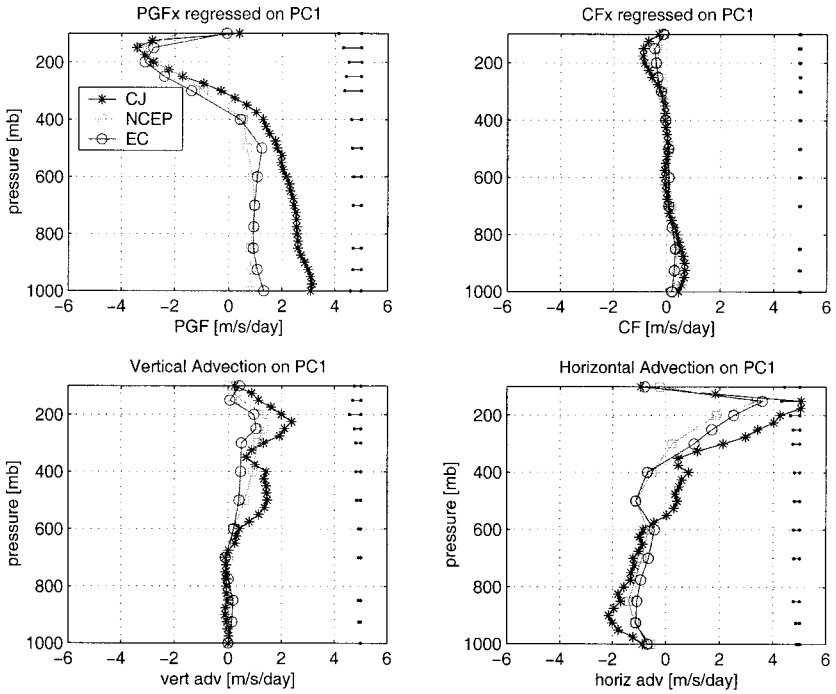

FIG. 9. Terms of IFA zonal momentum budget regressed onto PC1 of vector wind for IOP, normalized to correspond to 1 std dev anomaly of PC1 from its time mean. (clockwise from upper left) Pressure gradient force; Coriolis force; horizontal advection; and vertical advection. Error bars indicate 1 std dev difference between NCEP and ECMWF.

of conditions during WWBs, and an indication of the variation of cumulus momentum fluxes during the MJO.

The second EOF profile (not shown), which explains 17%–20% of the variance (depending on the analysis), has a nearly barotropic 2–4 m s^{-1} zonal anomaly. The meridional anomaly is again nearly zero at all levels. This pattern peaks in amplitude during November and early January, but the strongest signal is at timescales longer than the MJO.

The PC1-regressed profiles of zonal and meridional forcing are shown in Figs. 9 and 10, respectively. The local time rate of change terms are again negligible and are omitted. The large systematic error in the CJ time-mean meridional pressure gradient (Fig. 6) is not evident in the PC1 regression, except near the tropopause. However, the CJ regressed zonal pressure gradient is much larger than in the reanalyses, and is not balanced by any other term. Consequently, there is a large zonal residual throughout the troposphere in the CJ analysis (Fig. 11). This profile violates our consistency check, and suggests there are also significant time-varying errors in the CJ analysis.

The regressed reanalysis residuals are essentially indistinguishable from zero throughout the troposphere, except possibly at 1000 mb. However, agreement between the reanalyses is significantly improved over the time-mean case. In particular, the systematic differences seen between the mean pressure gradient profiles (Figs. 4 and 6) are not evident in the PC-regressed profiles (Fig. 9 and 10). The differences between the other regressed momentum terms are also smaller. This suggests that the differences between the reanalyses are largely time-independent, and that the strongest variability is common to both analyses.

In Fig. 5, we showed that the three analyses produced considerably different profiles of the mean vertical velocity. This contributed to corresponding differences in the mean vertical advection of momentum. In contrast, the time variation of vertical velocity is quite consistent between the three analyses (Fig. 12). All three analyses show that positive PC1 (low-level westerlies) corresponds to anomalous ascent in the upper troposphere with anomalous subsidence in the lower troposphere, as also found by Wang and Schlesinger (1999). This may correspond to a higher fraction of stratiform precipitation from extensive anvils associated with deep mesoscale convective systems. In the negative PC1 phase, convection is shallower and more localized with a less top-heavy heating profile.

c. Time-varying momentum budget—Estimating uncertainty

In order to assess the usefulness of reanalysis data for momentum budget calculations, we must have an estimate of the uncertainty in the budget residuals. Errors are estimated at all levels common to both reanalyses in the following way.

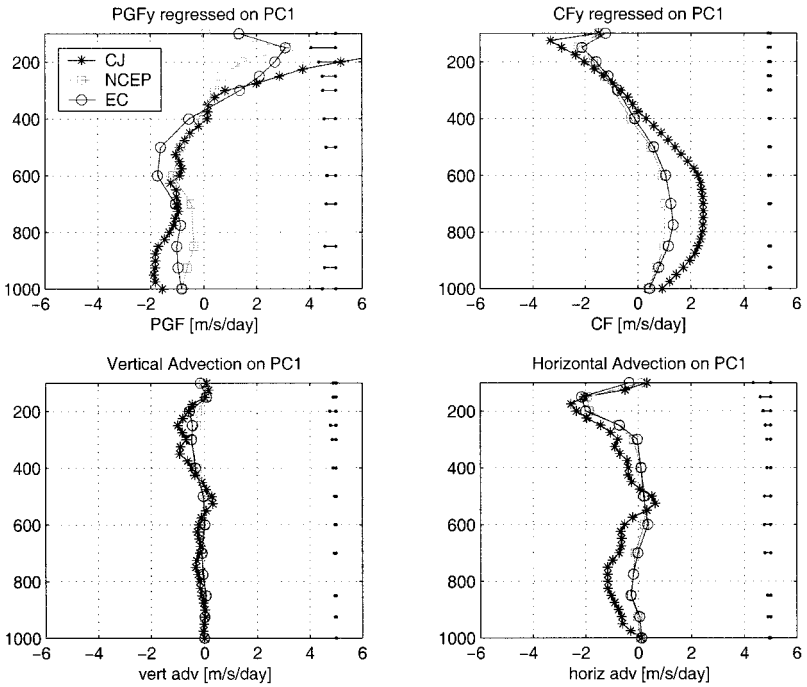

FIG. 10. Terms of IFA zonal momentum budget regressed onto PC1 of vector wind for IOP, normalized to correspond to 1 std dev anomaly of PC1 from its time mean. (clockwise from upper left) Pressure gradient force; Coriolis force; horizontal advection; and vertical advection. Error bars indicate 1 std dev difference between NCEP and ECMWF.

A 5-day-running-mean filter is applied to each term of the momentum equation for each analysis. The difference between ECMWF and NCEP is then calculated for corresponding times every fifth day to form an independent sample. The mean and standard deviation of these individual differences is shown in Fig. 13 for the zonal component. Contributions from the local time rate of change term are small, but nonnegligible, and are included in the residual error estimate below.

Systematic differences between the two analyses, given by the mean difference (open circels in Fig. 13), are evident in the pressure gradient term and at upper levels in the vertical advection term, as discussed in previous sections. Random errors, given by the standard deviation of the differences (dashed lines in Fig. 13), are (as expected) greatest in the pressure gradient term, but are also large at all levels in the horizontal advection term. This suggests that the timing of periods of strong horizontal advection may be disparate between the two analyses. This is investigated further in the following section.

Our estimate of the random uncertainty in the time-mean momentum terms is taken to be the standard deviation of the mean difference in each term (solid lines in Fig. 13 and error bars in Figs. 9 and 10). This is simply the standard deviation of the individual differences divided by the square root of the number of samples minus 1. We assume the random uncertainty in the PC1-regressed momentum terms is equal to the time-

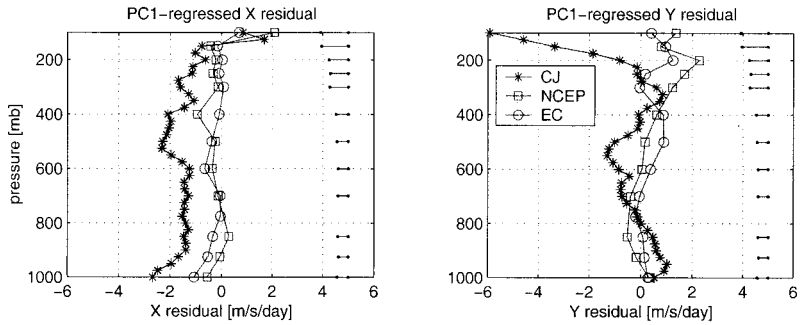

FIG. 11. IFA zonal and meridional budget residuals regressed onto PC1 of vector wind for IOP, normalized to correspond to 1 std dev anomaly of PC1 from its time mean. Error bars indicate 1 std dev difference between NCEP and ECMWF.

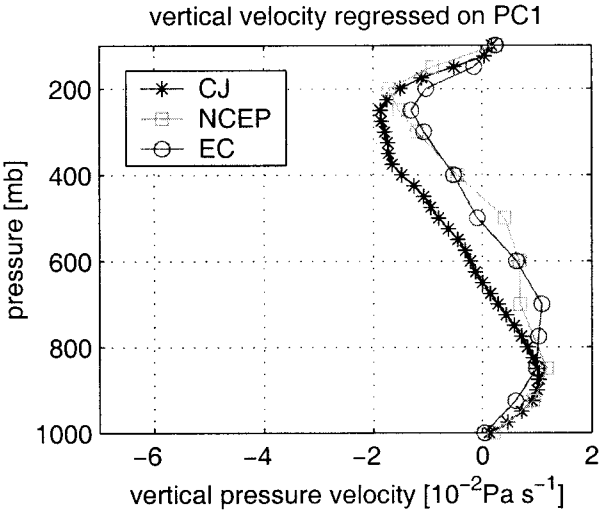

FIG. 12. IFA vertical pressure velocity regressed onto PC1 of vector wind for IOP, normalized to correspond to 1 std dev anomaly of PC1 from its time mean. Negative values indicate upward motion when PC1 is positive.

mean uncertainty. Meridional random uncertainty (not shown) is also largest in the pressure gradient and horizontal advection terms.

Five-day-running-mean random uncertainty in the zonal pressure gradient is about 1.5 m s^{-1} day^{-1} in the lower troposphere, while for horizontal advection it is about 0.5 m s^{-1} day^{-1}. In the upper troposphere uncertainty is larger in all terms. The resulting uncertainty in the 5-day-running-mean zonal residual, X, is 2.0 m s^{-1} day^{-1} in the lower troposphere and 3–5 m s^{-1} day^{-1} in the upper troposphere. Uncertainty in Y is slightly larger. Taking the 4-month average of all terms reduces the random X uncertainty to 0.5 m s^{-1} day^{-1} in the lower troposphere and 1.0 m s^{-1} day^{-1} in the upper troposphere, as shown in Fig. 11.

d. Time-varying momentum budget—Time series and correlation to convection

In the previous sections, we used averaging and compositing to construct momentum budgets with small random errors. However, since many other studies focus on specific periods of TOGA COARE, we investigate the viability of our analyses for constructing time series of cumulus momentum flux convergence.

Figure 14 gives the evolution of the zonal budget residual at selected levels during the IOP from NCEP and ECMWF, smoothed with a 5-day-running-mean filter. The zonal accelerations, X, due to momentum flux convergence are largest in the boundary layer (especially during the strong surface westerlies of days 355–370), and near the tropopause. Sustained accelerations of up to $X = 5$ m s^{-1} day^{-1} are also seen in the middle troposphere. These accelerations, if real, would damp

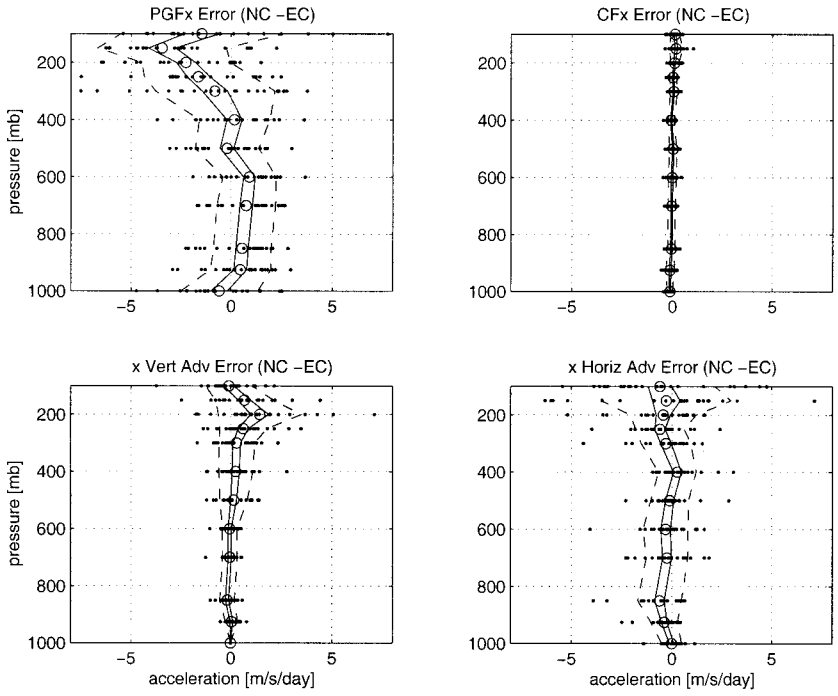

FIG. 13. Difference between ECMWF and NCEP reanalysis 5-day-running-mean zonal momentum terms for IFA region during IOP. Samples (solid dots) taken every fifth day. Open circles are sample mean for each vertical level. Dashed lines are sample std dev. Solid lines are std dev 4-month-mean terms. (clockwise from upper left) Pressure gradient force; Coriolis force; horizontal advection; and vertical advection.

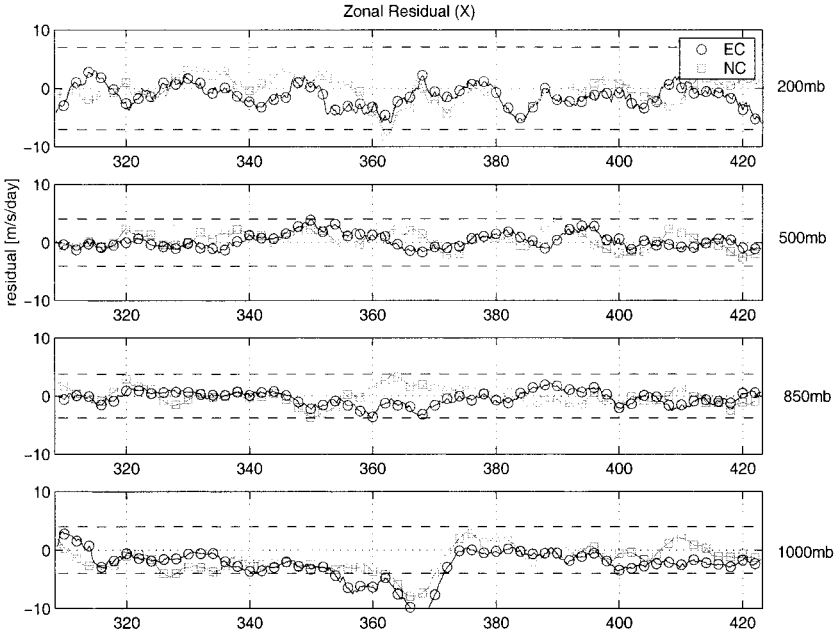

FIG. 14. Zonal budget residual averaged over IFA region during IOP and smoothed with 5-day-running-mean filter (data are plotted at 2-day intervals for clarity). (from top) At 200, 500, 850, and 1000 mb. Dashed lines correspond to 1 std dev 5-day-mean error bars.

out the deep tropospheric vertical shear in 5–10 days in the absence of other accelerations. However, large differences exist between the analyses. We now investigate the source of these differences.

Figure 15 gives the evolution of the zonal pressure gradient force. The onset of the day 367 WWB is accompanied by a strong (>10 m s^{-1} day^{-1} at 850 mb) lower-tropospheric eastward-directed pressure gradient acceleration in both reanalyses. Horizontal advection (Fig. 16) acts to accelerate the zonal flow in the opposite sense. However, the reanalyses differ substantially in the timing and magnitude of the increase in horizontal advection, especially at 850 mb. As a result, the character of the zonal residual (Fig. 14) during the onset of the WWB is in doubt. In NCEP, horizontal advection exceeds the pressure gradient acceleration at 850 mb, resulting in eastward residual acceleration ($X > 0$). In ECMWF the pressure term dominates and the 850-mb residual is negative.

The residuals also show large (>3 m s^{-1} day^{-1}) differences during several other periods at one or more levels. These differences are dominated by differences in the pressure gradient term. The pressure gradient discrepancies are frequently nonbarotropic, and therefore cannot be explained by surface pressure errors alone.

Error bars indicating the 5-day-running-mean X uncertainty at each level are given by the dashed lines. Only at the lowest levels, during the strongest event, does the signal clearly exceed the background noise. There is also no indication that residuals are larger during high-shear, high-precipitation periods.

4. Large-domain budgets

a. Minimizing pressure uncertainty—Central Pacific

Here we attempt to reduce the role of errors in the pressure gradient by averaging the forcing terms over a larger region of deep convection. We examine a section of the central Pacific 10°S–10°N, 160°E–140°W during the same 4-month period used for the IFA study. ECMWF (NCEP) precipitation averaged 8.3 (5.9) mm day^{-1} during the period, compared with 5.9 (7.7) mm day^{-1} in the IFA region.

Figure 17 gives the time-mean zonal and meridional wind components from each data set. Low-level winds are easterly in this region, with upper-level westerlies and weak meridional winds. The differences between the two analyses are considerably larger than in the COARE case. Although tropical atmosphere–ocean buoy wind observations cover the entire Pacific, anchoring the surface analysis, the additional upper-air observations taken during COARE in the IFA region clearly helped to constrain the analyses above the surface compared to the central Pacific case.

The terms of the momentum equation averaged over the 4 months are given in Figs. 18 and 19. Estimates of the random uncertainty in each term as determined by the method outlined in section 3c are also given. Despite the sparser observations, averaging over a larger domain reduces random and systematic differences between the analyses in both the zonal and meridional directions (cf. Fig. 4 and 6). Figure 20 shows that the

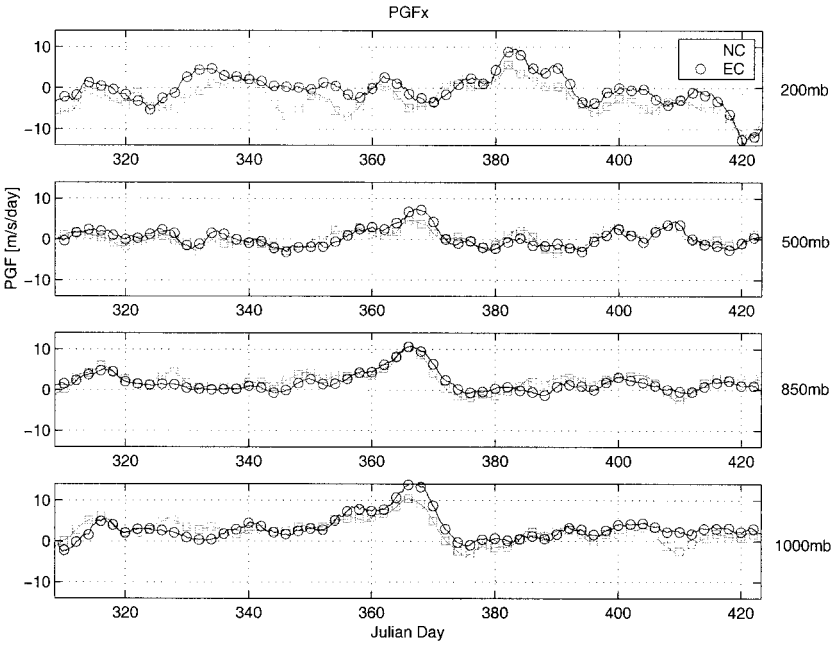

FIG. 15. Zonal pressure gradient force averaged over IFA region during IOP and smoothed with 5-day-running-mean filter (data are plotted at 2-day intervals for clarity). (from top) at 200, 500, 850, and 1000 mb.

resulting 4-month-mean random error in X is reduced to 0.2 m s^{-1} day^{-1} in the lower troposphere, or less than half the error in the IFA budget residual.

Again in the central Pacific case, X is a significant term below 850 mb. The ECMWF budget also suggests a role for cumulus transport near the tropopause. However, the residual is not significantly different from zero at these levels in the NCEP budget. In the meridional budget, the residual is only significant at the lowest level, but Y seems to decrease more rapidly with height

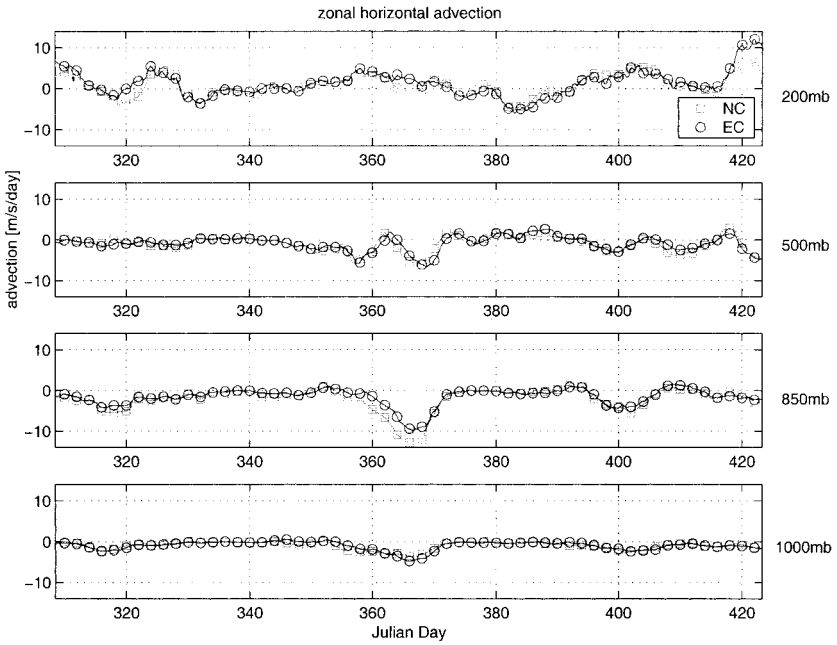

FIG. 16. Zonal horizontal advection averaged over IFA region during IOP and smoothed with 5-day-running-mean filter (data are plotted at 2-day intervals for clarity). (from top) at 200, 500, 850, and 1000 mb.

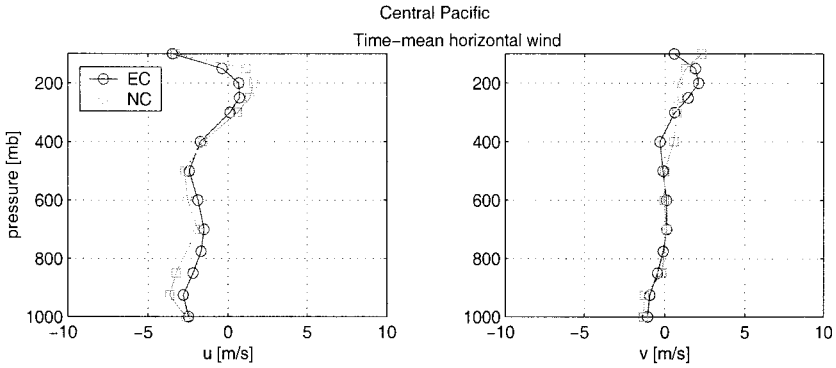

FIG. 17. Time-mean zonal and meridional wind components averaged over central Pacific region during IOP.

in the boundary layer than does *X*. Integrating the zonal residuals vertically (lower panels, Fig. 20), we again see more reasonable across tropopause fluxes in the ECMWF budget than in NCEP. But once again both analyses suggest a reduction in deep tropospheric zonal shear by CMT. The character of meridional fluxes is again ambiguous.

We also performed an EOF analysis like that for the IFA. The leading EOF and PC are similar to that for the IFA, and again the PC1-regressed budget residuals are essentially indistinguishable from zero at all levels despite substantial deep shear across the upper troposphere.

b. Test case—ITCZ

Given our success in reducing the pressure gradient errors in the central Pacific case, we construct a momentum budget for a yet larger region with substantial deep tropospheric shear and deep convection. We examine the region defined by 7.5° to 15.0°N and 175.0°E to 100.0°W during the same 4-month period used in previous sections. This region roughly defines the east Pacific ITCZ during this season.

The period is characterized by mean low-level easterlies and upper-level westerlies (Fig. 21, lower panels), with greater than 15 m s^{-1} of tropospheric zonal shear.

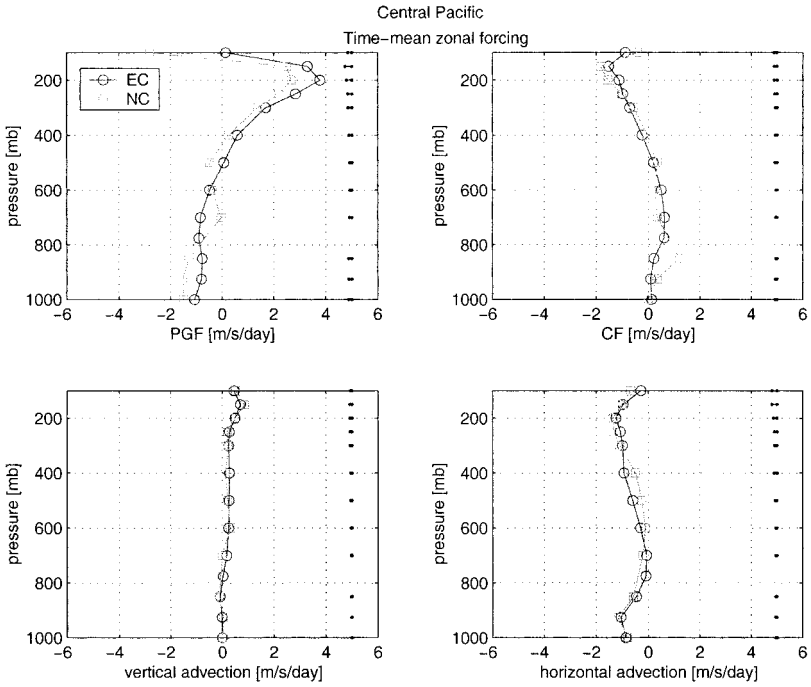

FIG. 18. Terms of time-mean zonal momentum budget averaged over central Pacific region during IOP. (clockwise from upper left) Pressure gradient force; Coriolis force; horizontal advection; and vertical advection. Error bars indicate 1 std dev difference between NCEP and ECMWF.

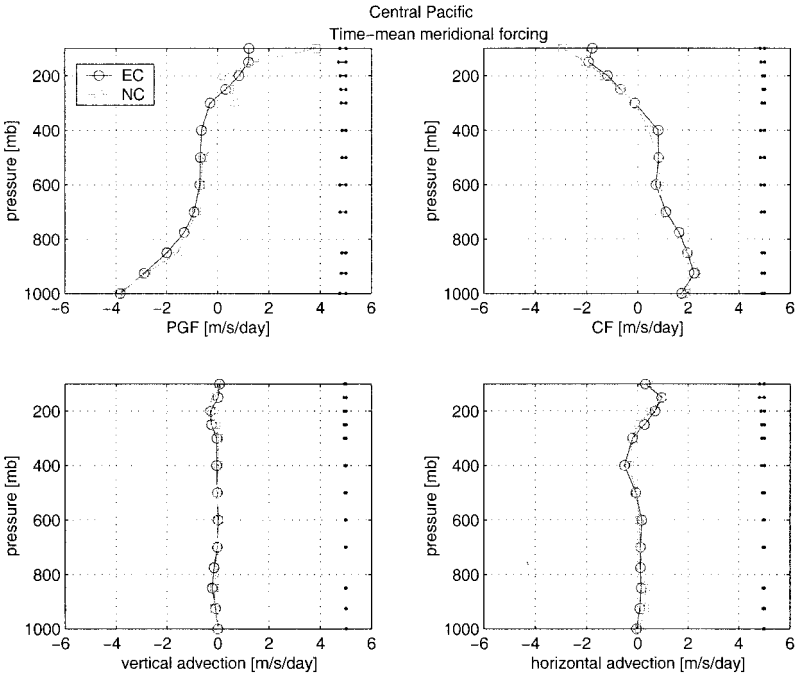

FIG. 19. Terms of time-mean meridional momentum budget averaged over central Pacific region during IOP. (clockwise from upper left) Pressure gradient force; Coriolis force; horizontal advection; and vertical advection. Error bars indicate 1 std dev difference between NCEP and ECMWF.

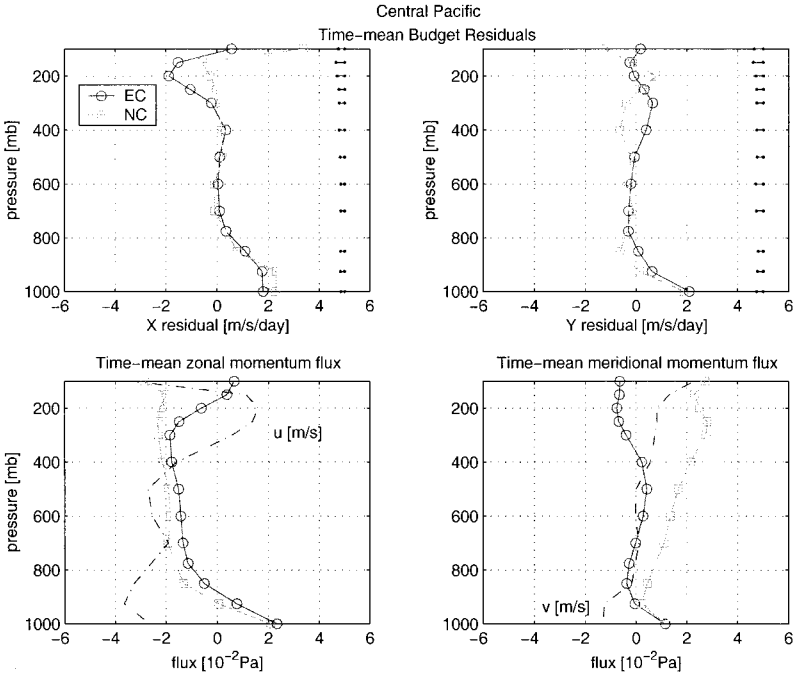

FIG. 20. (top) Time-mean zonal and meridional budget residuals, averaged over central Pacific region during IOP. Error bars indicate 1 std dev difference between NCEP and ECMWF. (bottom) Time-mean zonal and meridional wind components from NCEP, and momentum fluxes from ECMWF and NCEP, averaged over central Pacific region during IOP. Positive values indicate upward flux of westerly/southerly momentum.

Meridional winds are again relatively weak. Precipitation during the period is again comparable to the IFA. Mean ECMWF rainfall was 7.2 mm day^{-1}; NCEP was 5.7 mm day^{-1}.

Random errors in the time-mean zonal pressure gradient term (not shown) are again substantially reduced relative to the IFA budget. However, differences in the zonal Coriolis term are much larger than in either of the previous cases, and systematic meridional ECMWF–NCEP differences in the pressure gradient and Coriolis force are up to 10 m s^{-1} day^{-1}.

The source of these differences is almost certainly a discrepancy in the mean position of the ITCZ in the two models, which are constrained by very few observations in this region. Surprisingly, the budget residuals (Fig. 21, upper panels) show quite good agreement despite the model differences. Surface drag is again distributed up to 850 mb in the zonal direction, compared to 900 mb in the meridional direction. The zonal residual is again indistinguishable from zero above 850 mb. The resulting zonal flux profiles are also given in Fig. 21, and again indicate predominantly downgradient transport in the 4-month average. In the meridional direction, both reanalyses indicate a negative residual throughout the free troposphere, which produces unrealistic fluxes across the tropopause. The EOF analysis for the ITCZ region (not shown) gives a PC1 time series dominated by the seasonal shift in the zonal wind, rather than variability associated with the MJO.

5. Comparison with parameterizations

Finally, we compare the profiles of momentum flux convergence derived from the reanalysis budgets to those predicted by parameterizations of CMT. In this paper we consider the parameterizations of Schneider and Lindzen (1976) and Gregory et al. (1997). Both are mass-flux schemes, in which all air in the updraft or downdraft is assumed to have horizontally uniform properties.

These parameterizations rely on estimates of cumulus updraft and downdraft mass flux. To obtain these estimates we first calculate a cumulus contribution, ω_c, to the large-scale observed vertical velocity, ω, by subtracting an estimate of the environmental subsidence necessary to maintain a constant environmental temperature in the presence of radiative cooling, ω_{rc}:

$$\omega_c = \omega - \omega_{rc}. \tag{5}$$

We assume a mean tropospheric cooling rate of 10^{-5} K s^{-1}. The subsidence required to balance this cooling assuming an adiabatic lapse rate of 6 K km^{-1} is $\omega_{rc} = 1.6 \times 10^{-2}$ Pa s^{-1}.

From ω_c we obtain the net cumulus mass flux:

$$\omega_c = -g(M_u - M_d). \tag{6}$$

We solve for the updraft (subscript u) and downdraft (subscript d) mass flux, M, by assuming an updraft/downdraft mass flux ratio, $M_u/M_d = 2$ at all levels. This reasonably approximates the ratio found by Wu et al. (1998) in a 39-day cloud-resolving model (CRM) simulation of the period from day 340 to day 379. The updraft momentum flux can then be expressed as

$$-\left(\frac{1}{g}\right)\overline{u'\omega'}_u(p) = M_u(p)[u_u(p) - \overline{u}(p)]. \tag{7}$$

Here the overbar indicates environmental quantities. Primes are perturbations from environmental values. A similar calculation gives the downdraft momentum flux. Taking the derivative of the fluxes with respect to pressure gives the momentum flux convergence, X. Schneider and Lindzen (1976), (hereafter SL) assumed updraft air conserves its cloud-base momentum. Here we approximate cloud base momentum by the value at 925 mb, so that, for SL,

$$u_u(p) = \overline{u}\ (925\ \text{mb}). \tag{8}$$

The SL scheme does not take into account entrainment or across-updraft pressure gradients, and neglects downdraft effects.

The Gregory et al. (1997, hereafter G97) parameterization includes these process. Fluxes are computed using a form analogous to Eq. (7), but in Eq. (8) updraft momentum adjusts according to

$$\frac{\partial u_u}{\partial p} = \varepsilon_u[u_u - \overline{u}] + C\frac{\partial}{\partial p}\overline{u}, \tag{9}$$

where C is a coefficient determined empirically by Gregory et al. to be 0.7, and ε is an entrainment rate defined by

$$-\left(\frac{1}{M_u}\right)\frac{dM_u}{dp} = \varepsilon_u - \delta_u. \tag{10}$$

Here δ is a detrainment rate. Similar equations determine the downdraft momentum.

The entrainment/detrainment rate is determined by assuming that at any level the draft is either entraining or detraining, but not both. If the updraft mass flux is increasing with increasing elevation it is entraining ($\delta = 0$). If the updraft mass flux is decreasing with height it is detraining ($\varepsilon = 0$). The reverse is assumed for the downdraft.

Figure 22 gives the time-mean profiles of wind and momentum flux convergence from the ECMWF and NCEP budgets during the CRM simulation period. Also given are the X and Y profiles derived from the parameterization calculations, and from the CRM simulation itself. The period is dominated by a strong WWB event.

Above 850 mb, the agreement between all zonal profiles (with the exception of NCEP at 300 mb) is striking, with minima at 700 mb and near the tropopause, and a minimum at 500 mb. The G97 residual also agrees well in amplitude with the budget results above 850 mb. The SL scheme does not reproduce the amplitude as well.

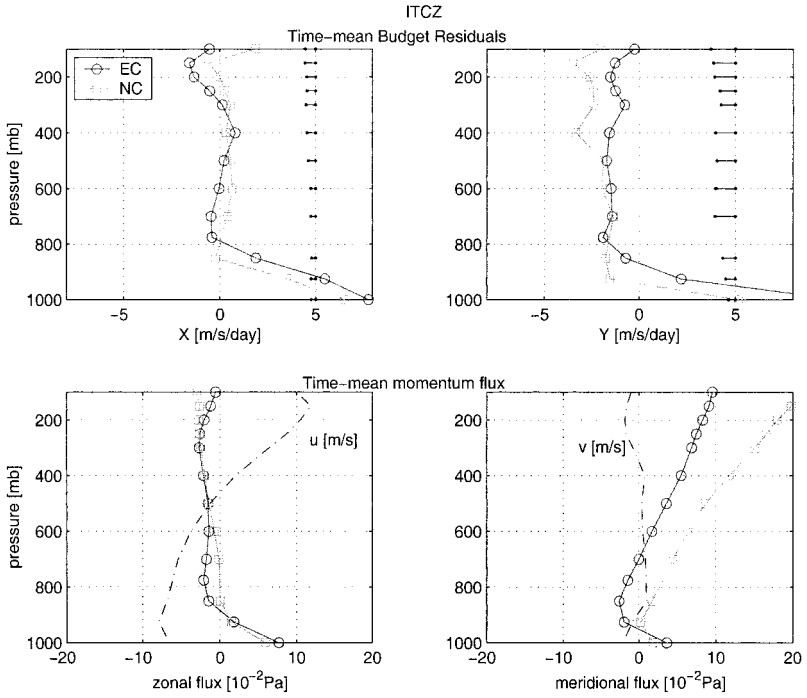

FIG. 21. (top) Time-mean zonal and meridional budget residuals, averaged over ITCZ region during IOP. Error bars indicate 1 std dev difference between NCEP and ECMWF. (bottom) Time-mean zonal and meridional wind components from NCEP, and momentum fluxes from NCEP and ECMWF, averaged over ITCZ region during IOP. Positive values indicate upward flux of westerly/southerly momentum.

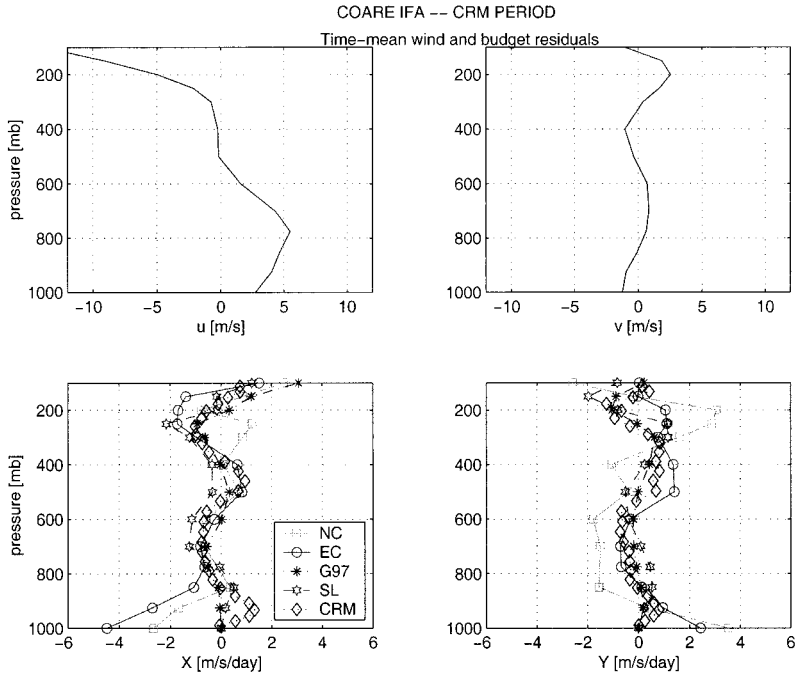

FIG. 22. (top) Time-mean zonal and meridional wind components averaged over IFA during 39-day CRM simulation, from ECMWF. (bottom) Time-mean zonal and meridional residuals averaged over IFA during CRM simulation, from NCEP budget (NC), ECMWF budget (EC), Gregory et al. parameterization (G97), Schneider and Lindzen parameterization (SL), and CRM simulation (CRM).

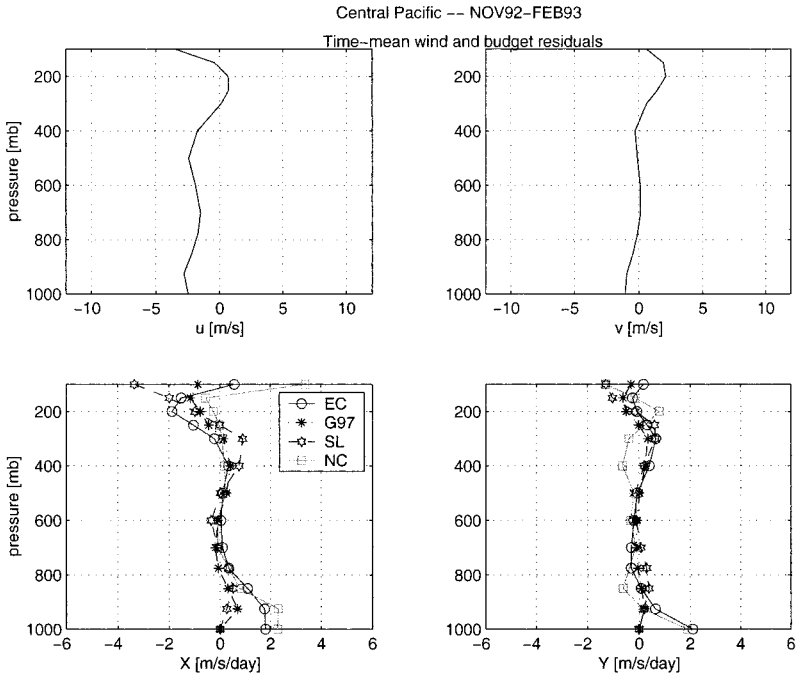

FIG. 23. (top) Time-mean zonal and meridional wind components averaged over central Pacific region during IOP, from ECMWF. (bottom) Time-mean zonal and meridional residuals averaged over central Pacific region during IOP, from ECMWF budget (EC), Gregory et al. parameterization (G97), Schneider and Lindzen parameterization (SL), and NCEP budget (NC).

At 500 mb, the SL scheme produces a residual of opposite sign to the budget residuals.

Below 850 mb, the model and budget residuals show large differences. The budget residuals indicate that subgrid-scale forcing is acting to decelerate the low-level westerlies. But neither the parameterization nor the CRM residuals have this character. In fact, the CRM indicates an enhancement of the low-level westerlies during this period.

Near the surface, it is likely not appropriate to attribute the budget residuals to CMT. Frictional drag is the more likely effect here. Since neither the parameterizations nor the CRM (which has a free-slip lower boundary condition) account for turbulent friction, this could account for the discrepancy with the budget profiles. However, the tropical turbulent mixed layer typically does not extend above 940 mb (Garstang and Betts 1974). The accelerations at 925 mb are therefore likely within the moist convective cloud layer.

If the budget 925-mb residuals are real, they therefore suggest that transport associated with moist convection is active in this layer. The sharp transition in the nature of the budget residuals at 850 mb argues a role for shallow-convective processes. Alternatively, it is possible that the reanalysis models are distributing the boundary layer drag above observed cloud base due to the models' coarse vertical resolution. However, the increase in the CJ objective analysis zonal residual below 850 mb (Fig. 7) supports the conclusion that the 925-mb reanalysis residuals are indeed due to moist convective transport.

Agreement in the meridional direction is not as good as in the zonal direction. The NCEP meridional budget is still plagued with pressure errors, but there is qualitative agreement between ECMWF and the models. Again the greatest difference is in the shallow convective boundary layer.

We can extend this method to the 4-month mean for the central Pacific region studied in section 4a. As mentioned, uncertainties in the budget residuals are much smaller for this case. Thus we can make a more certain assessment of the parameterizations. Parameterized profiles of X and Y for this region are given in Fig. 23. Once again we see qualitative agreement between the parameterizations and the budgets through most of the troposphere in the zonal direction. In the meridional direction, there is again qualitative agreement between ECMWF and the models, with NCEP as the outlier. As in the IFA case, large differences appear below 850 mb.

The agreement between ECMWF and the models may indicate that the small budget residuals at 200 and 400 mb in X, and at 300 mb in Y, are real. However, it is also possible the Tiedtke (1993) CMT parameterization in the ECMWF model, though somewhat different than the G97 scheme, is forcing the reanalysis residual toward a G97-like profile. The ECMWF scheme treats cloud-scale horizontal pressure gradients as a form of

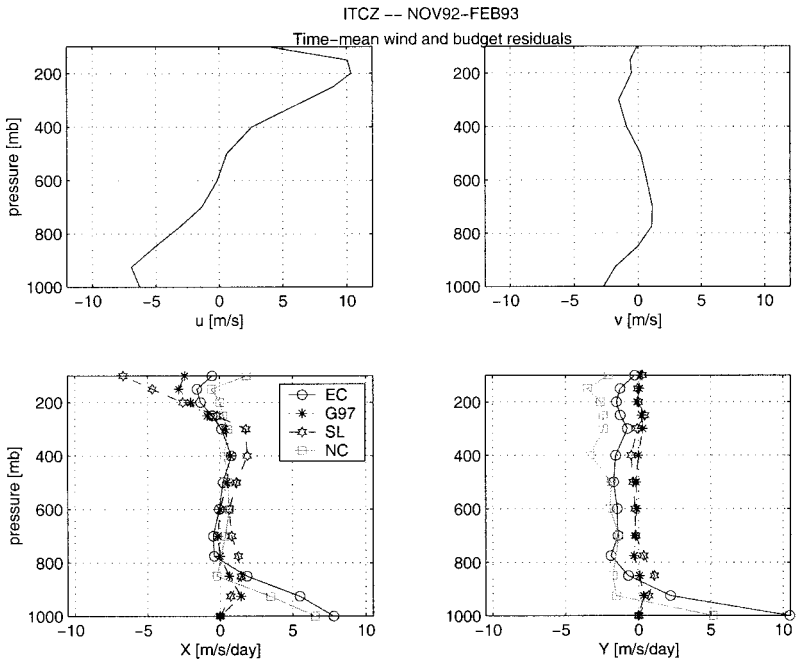

FIG. 24. (top) Time-mean zonal and meridional wind components averaged over ITCZ region during IOP, from ECMWF. (bottom) Time-mean zonal and meridional residuals averaged over ITCZ during IOP, from ECMWF budget (EC), Gregory et al. parameterization (G97), Schneider and Lindzen parameterization (SL), and NCEP budget (NC).

enhanced lateral entrainment, while G97 relates them to the vertical shear.

Finally, we examine the parameterizations over the ITCZ region. The random uncertainties in this region are larger than in the central Pacific case, but the deep-tropospheric shear is the strongest of any of the cases. The reanalysis and parameterized residuals are given in Fig. 24. Again we see qualitative agreement above 850 mb between the reanalyses and the parameterizations in the zonal direction. The meridional component has a large imbalance in both budgets. As in the IFA case, G97 matches the reanalysis more closely than SL in the zonal direction.

6. Summary and discussion

We studied convective momentum transport deduced from momentum budget calculations from the ECMWF and NCEP reanalyses over several tropical convective regions, including the TOGA COARE intensive flux array. The reanalyses showed good agreement with each other, and with an independent objective analysis for TOGA COARE, in terms derived from the directly observed horizontal winds (Coriolis force and horizontal advection). However, substantial differences were seen in the 4-month-mean vertical advection and pressure gradient terms. Large differences between the objective analysis and the reanalyses were also seen in the time-varying budget.

An error in the surface pressure at one of the sounding stations contaminated the objective analysis, and possibly to a lesser extent the 4-month-mean meridional pressure gradient force in the NCEP reanalysis, but the pressure gradient profiles regressed on the leading mode of wind variability (PC1), which is associated mainly with the MJO, were quite similar in the two reanalyses.

The time-mean meridional budget residual, Y, was essentially indistinguishable from zero except at the lowest level. But the time-mean zonal residual, X, was clearly a significant term in the budget below 850 mb, with accelerations up to 2 m s^{-1} day^{-1} in both reanalyses.

Analysis of the time-varying component of the budget found that the reanalyses differed substantially in the timing and magnitude of increases in horizontal advection during the onset of WWBs, and frequently contained large nonbarotropic pressure gradient differences, leading to large ''random'' differences between their budget residuals. The resulting uncertainty in the 5-day-mean zonal residual, X, was 2.0 m s^{-1} day^{-1} in the lower troposphere and 3-5 m s^{-1} day^{-1} in the upper troposphere. Uncertainty in Y was slightly larger. Taking the 4-month average of all terms reduced the random X error to 0.5 m s^{-1} day^{-1} in the lower troposphere and 1.0 m s^{-1} day^{-1} in the upper troposphere.

Budget residuals above 850 mb were not clearly detectable above the uncertainty. However, the zonal time-mean momentum flux profiles from both reanalyses suggested a preference for downgradient transport.

Similar results were obtained from momentum bud-

gets constructed for larger domains in the central and eastern tropical Pacific. Random and systematic differences between the analyses averaged over these larger domains were clearly reduced in both the zonal and meridional directions. In particular, uncertainty in the zonal pressure gradient was halved.

The residual profiles were compared with predictions of two CMT parameterization schemes and a CRM during the December–January IFA westerly wind burst. Despite the smallness of the residuals, they were in good agreement with the Gregory et al. (1997) CMT scheme, and with the CRM, above 850 mb. The Gregory et al. scheme also agreed well with the ECMWF residuals of the central and eastern Pacific budgets. Agreement with the Schneider–Lindzen (1976) scheme was somewhat less favorable. Both parameterizations, and the CRM, failed to capture large residuals in the shallow-convective boundary layer.

This study indicates that estimates of cumulus momentum fluxes from large-scale observations contain substantial uncertainty, even given a high quality, intensive dataset such as TOGA COARE. While noisy, however, the residual profiles are surprisingly consistent with the Gregory et al. scheme above 850 mb. The differences between the budget residuals and the models below 850 mb demonstrate the need to better assess momentum transport in the lower troposphere, particularly momentum mixing by shallow cumulus.

It would also be interesting to use reanalyses to examine CMT in other regions of organized convection (e.g., African easterly waves, or summertime continental convective outbreaks), as well as in understanding its role in the Hadley and Walker circulations.

Acknowledgments. Our thanks to Paul Ciesielski for provision and interpretation of objective analysis data, Dave Gregory and Ernst Klinker for their insights into the ECMWF reanalysis, Xiaoqing Wu for the use of his CRM data, and Marc Michelsen for his technical expertise. Thanks also to Michio Yanai, Wen-wen Tung, and Brain Mapes for invaluable conversations, and to Kevin Werner for his help in revising the manuscript. This work was supported by NSF Grant ATM-9877021.

REFERENCES

Brown, A. R., 1999: Large-eddy simulation and parameterization of the effects of shear on shallow cumulus convection. *Bound.-Layer Meteor.,* **91,** 65–80.

Ciesielski, P. E., L. M. Hartten, and R. H. Johnson, 1997: Impacts of merging profiler and rawinsonde winds on TOGA COARE analyses. *J. Atmos. Oceanic Technol.,* **14,** 1264–1279.

Flatau, M., and D. E. Stevens, 1987: The effect of horizontal pressure gradients on the momentum transport in tropical convective lines. Part II: Lagrangian calculations. *J. Atmos. Sci.,* **44,** 2088–2096.

Gallus, W. A., Jr., and R. H. Johnson, 1992: The momentum budget of an intense midlatitude squall line. *J. Atmos. Sci.,* **49,** 422–450.

Gao, K., D.-L. Zhang, M. W. Moncrieff, and H.-R. Cho, 1990: Mesoscale momentum budget of a midlatitude squall line: A numerical case study. *Mon. Wea. Rev.,* **118,** 1011–1028.

Garstang, M., and A. K. Betts, 1974: Review of the tropical boundary layer and cumulus convection: Structure, parameterization, and modeling. *Bull. Amer. Meteor. Soc.,* **55,** 1195–1205.

Gibson, J. K., P. Kållberg, S. Uppala, A. Hernandez, A. Nomura, and E. Serrano, 1997: *ERA description.* ECMWF Reanalysis Project Report Series, Vol. 1, ECMWF, 72 pp.

Gregory, D., R. Kershaw, and P. M. Inness, 1997: Parameterization of momentum transport by convection. II: Tests in single column and general circulation models. *Quart. J. Roy. Meteor. Soc.,* **123,** 1153–1183.

Holland, J. Z., and E. M. Rasmussen, 1973: Measurements of the atmospheric mass, moisture and momentum budgets over a 500-kilometer square of tropical ocean. *Mon. Wea. Rev.,* **101,** 44–55.

Holton, J. R., 1992: *An Introduction to Dynamic Meteorology.* Academic Press, 511 pp.

Houze, R. A., Jr., 1973: A climatological study of vertical transports by cumulus-scale convection. *J. Atmos. Sci.,* **30,** 1112–1123.

Inness, P. M., and D. Gregory, 1997: Aspects of the intraseasonal oscillation simulated by the Hadley Centre Atmospheric Model. *Climate Dyn.,* **13,** 441–458.

Kain, J. S., and J. M. Fritsch, 1990: A one-dimensional entraining/detraining plume model and its application in convective parameterization. *J. Atmos. Sci.,* **47,** 2784–2802.

Kalney, E., and Coauthors, 1996; The NCEP/NCAR 40-Year Reanalysis Project. *Bull. Amer. Meteor. Soc.,* **77,** 437–471.

Kershaw, R., and D. Gregory, 1997: Parametrization of momentum transports by convection. I: Theory and cloud modeling results. *Quart. J. Roy. Meteor. Soc.,* **123,** 1133–1151.

Kiehl, J. T., J. J. Hack, G. B. Bonan, B. A. Boville, B. P. Briegleb, D. L. Williamson, and P. J. Rasch, 1996: Description of the NCAR Community Climate Model (CCM3). NCAR Tech. Note NCAR/TN−420+STR, 152 pp. [Available from NCAR, Boulder, CO 80307.]

LaFore, J.-P., J.-L. Redelsperger, and G. Jaubert, 1988: Comparison between a three-dimensional simulation and Doppler radar data of a tropical squall line: Transport of mass, momentum and moisture. *J. Atmos. Sci.,* **45,** 3483–3500.

LeMone, M. A., 1983: Momentum transport by a line of cumulonimbus. *J. Atmos. Sci.,* **40,** 1815–1834.

——, and D. P. Jorgenson, 1991: Precipitation and kinematic structure of an oceanic mesoscale convective system. Part II: Momentum transport and generation. *Mon. Wea. Rev.,* **119,** 2638–2653.

——, and M. W. Moncrieff, 1993: Momentun transport by convective bands: Comparisons of highly idealized dynamical models to observations. *The Representation of Cumulus Convection in Numerical Models, Meteor. Monogr.,* No. 46, Amer. Meteor. Soc., 75–92.

——, G. M. Barnes, and E. J. Zipser, 1984: Momentum flux by lines of cumulonimbus over the tropical oceans. *J. Atmos. Sci.,* **41,** 1914–1932.

Lin, X., and R. H. Johnson, 1996: Heating, moistening, and rainfall over the western Pacific warm pool during TOGA COARE. *J. Atmos. Sci.,* **53,** 3367–3383.

Moncrieff, M. W., 1992: Organized convective systems: Archetypal dynamical models, mass and momentum flux theory, and parameterization. *Quart. J. Roy. Meteor. Soc.,* **118,** 819–850.

Schneider, E. K., and R. S. Lindzen, 1976: A discussion of the parameterization of momentum exchange by cumulus convection. *J. Geophys. Res.,* **81,** 3158–3180.

——, and ——, 1977: Axially symmetric steady-state models of the basic state for instability and climate studies. Part I. Linearized calculations. *J. Atmos. Sci.,* **34,** 263–279.

Soong, S.-T., and W.-K. Tao, 1984: A numerical study of the vertical transport of momentum in a tropical rainband. *J. Atmos. Sci.,* **41,** 1049–1061.

Stevens, D., 1979: Vorticity, momentum, and divergence budgets of synoptic-scale wave disturbances in the tropical eastern Atlantic. *Mon. Wea. Rev.,* **107,** 535–550.

Sui, C.-H., and M. Yanai, 1986: Cumulus ensemble effects on the large-scale vorticity and momentum fields of GATE. Part I: Observational evidence. *J. Atmos. Sci.,* **43,** 1618–1642.

Tiedtke, M., 1993: Representation of clouds in large-scale models. *Mon. Wea. Rev.,* **121,** 3040–3061.

Trier, S. B., M. A. LeMone, and W. C. Skamarock, 1998: Effect of three-dimensional structure on the stormwide horizontal accelerations and momentum budget of a simulated squall line. *Mon. Wea. Rev.,* **126,** 2580–2598.

Wang, W., and M. E. Schlesinger, 1999: The dependence on convection parameterization of the tropical intraseasonal oscillation simulated by the UIUC 11-layer atmospheric GCM. *J. Climate,* **12,** 1423–1457.

Webster, P. J., and R. Lukas, 1992: TOGA COARE: The Coupled Ocean–Atmosphere Response Experiment. *Bull. Amer. Meteor. Soc.,* **73,** 1377–1416.

Wu, X., and M. Yanai, 1994: Effects of vertical wind shear on the cumulus transport of momentum: Observations and parameterization. *J. Atmos. Sci.,* **51,** 1640–1660.

——, W. W. Grabowski, and M. W. Moncrieff, 1998: Long-term behavior of cloud systems in TOGA COARE and their interactions with radiative and surface processes. Part I: Two-dimensional modeling study. *J. Atmos. Sci.,* **55,** 2693–2714.

Zhang, G. J., and H. R. Cho, 1991a: Parameterization of the vertical transport of momentum by cumulus clouds. Part I: Theory. *J. Atmos. Sci.,* **48,** 1483–1492.

——, and ——, 1991b: Parameterization of the vertical transport of momentum by cumulus clouds. Part II: Application. *J. Atmos. Sci.,* **48,** 2448–2457.

——, and N. A. McFarlane, 1995: Role of convective-scale momentum transport in climate simulation. *J. Geophys. Res.,* **100,** 1417–1426.